Hindawi
Journal of Robotics
Volume 2023, Article ID 8229356, 12 pages
https://doi.org/10.1155/2023/8229356

Research Article

Numerical Analysis of a TCR Adaptive to Different Tree Diameters for Unstructured Forest Environment: A TCR of Variable Diameter with Different Tree Diameters

Zhe Wu, Xigui Wang, and Zhiqin Zhang

School of Engineering Technology, Northeast Forestry University, No. 26, Hexing Road, Xiangfang District, Harbin 150040, China

Correspondence should be addressed to Xigui Wang; wyr20091207@126.com

Received 20 December 2022; Revised 20 January 2023; Accepted 27 January 2023; Published 16 February 2023

Academic Editor: Shuofei Yang

This paper proposes the optimal design and simulation analysis of a robot for tree-climbing, which has the ability to climb up the tree trunk to adapt to different tree diameter changes. In an unstructured forest environment, considering that the Tree-Climbing Robot (TCR) may collide with branches, reducing the success rate of tree climbing, the mechanical structure and movement strategy to avoid branches are predesigned. The presented TCR mimics several design principles that have been adapted to arboreal animals, including claw-hand grasping and climbing gait movements, and is optimally designed to achieve high manoeuvrability on irregularly shaped trees. Based on the *D-H* parameterization method, the kinematics model of the TCR is developed and its kinematic equations are solved. The accuracy of the kinematic equations is verified by MATLAB, and the reachable area of the working space of the manipulator of the TCR is determined. Using ADAMS to analyse the kinematics and dynamics of the climbing process of the TCR, the rationality of the gait planning of the robot is verified, and the time-varying characteristic curves of each physical quantity of each structural joint are derived and further simulated through numerical analysis, the results of which will profoundly validate the technical feasibility and design innovation of this presented TCR.

1. Introduction

Climbing robot is a challenging research topic, which has attracted the extensive attention of many scientific and technological researchers [1–3]. Most of such robots reported in the literature are designed for climbing on artificial structures, with only a few designed for climbing unstructured forest natural environments, such as trees [4–6]. Trees and man-made structures are very different in nature. This brings different technical challenges to the optimal design of climbing robots. A new type of Tree Climbing Robot (TCR) adapted to different tree diameters has been developed, which has achieved some breakthrough performance in avoiding branches and can complete various actions that are impossible for the most advanced TCRs, such as moving between the trunk and branches. The TCR proposed in this paper integrates cutting-edge technology fields and animal climbing methods and lays the foundation for subsequent analysis of such TCR sensing methods, environmental cognition, path planning, and motion planning in known and unknown environments. Based on the accumulation and precipitation of preresearch, this research provides a valuable reference for such robot designers to choose the appropriate climbing method when designing a TCR for a specific application.

TCRs are an important branch of agricultural and forestry robots and an important part of "Agriculture 4.0," and have become a research hotspot in scientific research institutions [7–9]. Agriculture 4.0 is derived from the concept of Industry 4.0, integrating computing, image processing, automation, machine vision, machine learning, and the intersection of big data and the Internet of Things [10]. Forestry is an extremely important part of Agriculture 4.0 and will be one of the broadest and most potential new application areas for robots in the future. In the field of agricultural and forestry robots, the research and

development of fruit and vegetable farmland planting, detection, and picking robots and drones has been relatively mature [11–13]. However, in the field of forest aviation operations, due to factors such as the complex high-altitude forest environment and the difficulty of research and development, there are few related robots. The existing robots in this field have a low level of automation and mechanization, and their operational efficiency is not high [14].

Forest aerial work, including fruit picking, branch pruning, ground quality monitoring, forest environment monitoring, and pest control, is done at high altitudes in dangerous environments with high complexity and danger, reflecting the greater demand for such TCRs [15]. The variability of forest tree diameter is an important reason affecting the development of TCR technology. The extremely complex tree surface profile and variable clamping diameter lead to the need for robots to switch climbing structures or methods from time to time [16–18]. At present, there are three main types of TCRs: wrap-around TCRs, gripping TCRs, and bionic TCRs. Compared with the wrap-around TCR, the clip-type TCR and the bionic TCR have the characteristics of simple structure, strong obstacle-surmounting ability, and high flexibility. Compared with the bionic TCR, the clip-type TCR has the characteristics of strong stability and strong load capacity [19–21]. Based on this, this paper develops a TCR with strong climbing ability, a variable diameter to adapt to various tree diameters, and the ability to complete different predetermined tasks.

Most of the above TCRs have complex structures and suffer from two major problems: difficulty crossing barriers and clamping invariant paths, which cannot adapt to complex forestry operating environments. To address the shortcomings of the above research, this paper proposes a variable-diameter, rotatable TCR, establishes a *D-H* parametric model of the TCR, solves its positive kinematic equations, verifies the correctness of the kinematics, and validates it through MATLAB simulations. The kinematic analysis and workspace of the TCR are analysed by combining kinematics and MATLAB to solve for the reachable area of the robot's workspace, which provides analytical data and a theoretical basis for subsequent TCR interference judgement and barrier crossing analysis.

2. Mechanism Design for Kinematic Analysis

The main structure of the TCR is designed with reference to climbing animals such as monkeys and koalas that have adapted to arboreal habitats. Figure 1 illustrates the general mechanical structure of the TCR, which consists of an upper clamping structure, a rotating body structure, a lower clamping structure, and a lifting structure. The main structure of the TCR has three rotational joints: the large arm joint, the small arm joint, and the rotating body joint, as well as one translational joint: the lifting joint. The TCR designed in this paper has a left-right symmetrical structure, with the large and small arm joints and the rotating body joints of the robot arm having rotational degrees of freedom and the ball screw being the degree of freedom of movement. Figure 1 illustrates the designed structure of a variable diameter TCR. Figure 2 describes the coordinate system of the TCR. Kinematic analysis is a basic task in tree-climbing robot modeling. Robot kinematics includes forward kinematics and inverse kinematics [22]. Forward kinematics analysis calculates the position and orientation of the end effector based on geometric parameters and joint angles [23]. Inverse kinematics analysis calculates joint angles based on the position and orientation of the end effector [24]. Kinematic analysis can form the basis for control and future optimization. The kinematic analysis of the TCR designed in this study includes forward kinematics solution, kinematics simulation verification, and workspace analysis. Considering the working range and motion state description of the TCR, the kinematics of the TCR are analysed, the main structure of the TCR is simplified into a series of link joints, and a joint coordinate system is established at each joint.

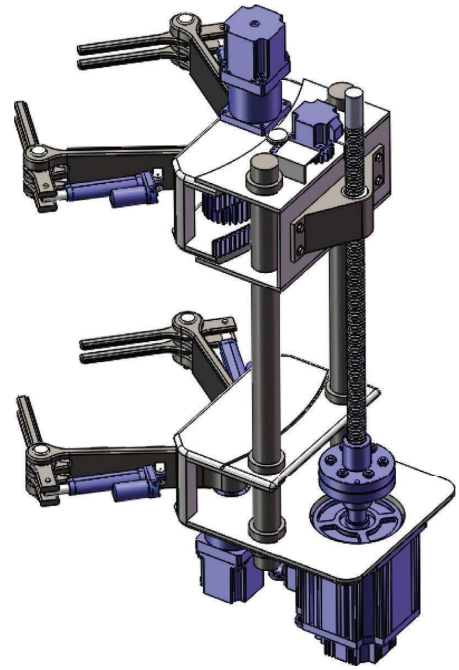

Figure 1: Designed structure of a variable diameter TCR.

As can be seen from Figure 2, $O - x_0 y_0 z_0$ is the world coordinate system. $O - x_{10} y_{10} z_{10}$ is the end effector coordinate system. For tree-climbing robots, $a1 = 202.49\,\text{mm}$, $a2 = 26\,\text{mm}$ $a3 = 193.84\,\text{mm}$, and $d \in [28, 278]\,\text{mm}$. According to the *D-H* matrix method, from left to right principle, the following is written as [25]:

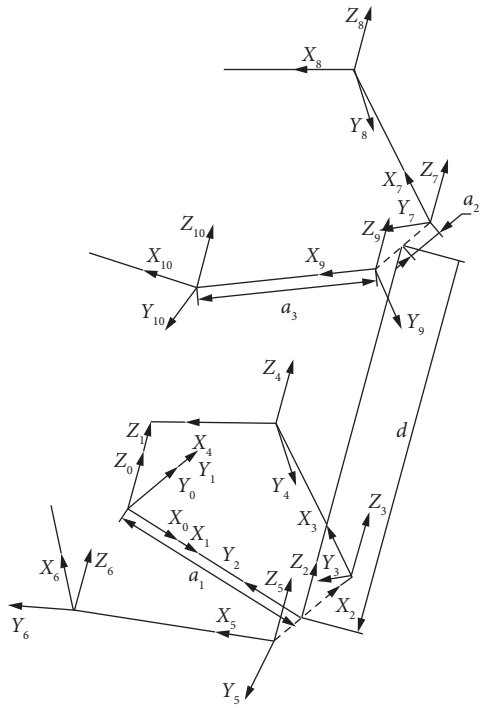

Figure 2: The coordinates system of the TCR.

$$
\begin{aligned}
{}_{i}^{i-1}T &= \mathrm{Rot}_X(\alpha_{i-1})\mathrm{Trans}_X(a_{i-1})\mathrm{Rot}_Z(\theta_i)\mathrm{Trans}_Z(d_i),\\
&= \begin{bmatrix} c\theta_i & -s\theta_i & 0 & a_{i-1} \\ s\theta_i c\alpha_{i-1} & c\theta_i c\alpha_{i-1} & -s\alpha_{i-1} & -s\alpha_{i-1}d_i \\ s\theta_i s\alpha_{i-1} & c\theta_i s\alpha_{i-1} & c\alpha_{i-1} & c\alpha_{i-1}d_i \\ 0 & 0 & 0 & 1 \end{bmatrix},
\end{aligned} \tag{1}
$$

where $c\theta_i$ represents $\cos\theta_i$ and $s\theta_i$ is shown as $\sin\theta_i$, multiplied by ${}_{i}^{i-1}T\,(i = 1, 2, \ldots, n)$ and according to the parameters in Table 1, which is written as

$$
{}_{1}^{0}T = \begin{bmatrix} \cos\theta_1 & -\sin\theta_1 & 0 & 0 \\ \sin\theta_1 & \cos\theta_1 & 0 & 0 \\ 0 & 0 & 1 & 0 \\ 0 & 0 & 0 & 1 \end{bmatrix},
$$

$$
{}_{2}^{1}T = \begin{bmatrix} 0 & -1 & 0 & a_1 \\ 1 & 0 & 0 & 0 \\ 0 & 0 & 1 & 0 \\ 0 & 0 & 0 & 1 \end{bmatrix},
$$

$$
{}_{3}^{2}T = \begin{bmatrix} \cos\theta_2 & -\sin\theta_2 & 0 & a_2 \\ \sin\theta_2 & \cos\theta_2 & 0 & 0 \\ 0 & 0 & 1 & 0 \\ 0 & 0 & 0 & 1 \end{bmatrix},
$$

$$
{}_{4}^{3}T = \begin{bmatrix} \cos\theta_3 & -\sin\theta_3 & 0 & a_3 \\ \sin\theta_3 & \cos\theta_3 & 0 & 0 \\ 0 & 0 & 1 & 0 \\ 0 & 0 & 0 & 1 \end{bmatrix}. \tag{2}
$$

The pose transformation matrix from coordinate system 4 to the base coordinate system is

$$
\begin{cases} {}_{4}^{0}T = {}_{1}^{0}T\,{}_{2}^{1}T\,{}_{3}^{2}T\,{}_{4}^{3}T, {}_{8}^{0}T = {}_{1}^{0}T\,{}_{2}^{1}T\,{}_{7}^{2}T\,{}_{8}^{7}T, {}_{6}^{0}T = {}_{1}^{0}T\,{}_{2}^{1}T\,{}_{5}^{2}T\,{}_{6}^{5}T, {}_{10}^{0}T = {}_{1}^{0}T\,{}_{2}^{1}T\,{}_{9}^{2}T\,{}_{10}^{9}T. \end{cases} \tag{3}
$$

Herein, the kinematic equation is expressed as follows:

Table 1: The link parameters of TCR.

i	a_{i-1}	α_{i-1}	d_i	θ_i
1	0	0	0	θ_1
2	a_1	0	0	90
3	a_2	0	0	θ_2
4	a_3	0	0	θ_3
5	$-a_2$	0	0	θ_4
6	a_3	0	0	θ_5
7	a_2	0	d	θ_6
8	a_3	0	0	θ_7
9	$-a_2$	0	d	θ_8
10	a_3	0	0	θ_9

$$
{}^{0}_{n}T = \begin{bmatrix} n_x & o_x & a_x & P_x \\ n_y & o_y & a_y & P_y \\ n_z & o_z & a_z & P_z \\ 0 & 0 & 0 & 1 \end{bmatrix}. \tag{4}
$$

Simultaneous equations, (2)–(4), are written as

$$
\begin{cases}
n_x = \sin\theta_9 \cdot (\sin\theta_1 \cdot \sin\theta_8 - \cos\theta_1 \cdot \cos\theta_8) - \cos\theta_9 \cdot (\cos\theta_1 \cdot \sin\theta_8 + \sin\theta_1 \cdot \cos\theta_8), \\
n_y = -\cos\theta_9 \cdot (\sin\theta_1 \cdot \sin\theta_8 - \cos\theta_1 \cdot \cos\theta_8) - \sin\theta_9 \cdot (\cos\theta_1 \cdot \sin\theta_8 + \cos\theta_8 \cdot \sin\theta_1), \\
n_z = 0, \\
o_x = \cos\theta_9 \cdot (\sin\theta_1 \cdot \sin\theta_8 - \cos\theta_1 \cdot \cos\theta_8) + \sin\theta_9 \cdot (\cos\theta_1 \cdot \sin\theta_8 + \cos\theta_8 \cdot \sin\theta_1), \\
o_y = \sin\theta_9 \cdot (\sin\theta_1 \cdot \sin\theta_8 - \cos\theta_1 \cdot \cos\theta_8) - \cos\theta_9 \cdot (\cos\theta_1 \cdot \sin\theta_8 + \sin\theta_1 \cdot \cos\theta_8), \\
o_z = 0, \\
a_x = 0, \\
a_y = 0, \\
a_z = 1, \\
p_x = a_1 \cdot \cos\theta_1 - a_3 \cdot (\cos\theta_1 \cdot \sin\theta_8 + \cos\theta_8 \cdot \sin\theta_1) + a_2 \cdot \sin\theta_1, \\
p_y = -a_3 \cdot (\sin\theta_1 \cdot \sin\theta_8 - \cos\theta_1 \cdot \cos\theta_8) - a_2 \cdot \cos\theta_1 + a_1 \cdot \sin\theta_1, \\
p_z = d.
\end{cases} \tag{5}
$$

Similarly, the numerical expression of each element in coordinate system 8 is shown as

$$\begin{cases} n_x = -\cos\theta_7 \cdot (\cos\theta_1 \cdot \sin\theta_6 + \cos\theta_6 \cdot \sin\theta_1) - \sin\theta_7 \cdot (\cos\theta_1 \cdot \cos\theta_6 - \sin\theta_1 \cdot \sin\theta_6), \\ n_y = \cos\theta_7 \cdot (\cos\theta_1 \cdot \cos\theta_6 - \sin\theta_1 \cdot \sin\theta_6) - \sin\theta_7 \cdot (\cos\theta_1 \cdot \sin\theta_6 + \cos\theta_6 \cdot \sin\theta_1), \\ n_z = 0, \\ o_x = \sin\theta_7 \cdot (\cos\theta_1 \cdot \sin\theta_6 + \cos\theta_6 \cdot \sin\theta_1) - \cos\theta_7 \cdot (\cos\theta_1 \cdot \cos\theta_6 - \sin\theta_1 \cdot \sin\theta_6), \\ o_y = -\cos\theta_7 \cdot (\cos\theta_1 \cdot \sin\theta_6 + \cos\theta_6 \cdot \sin\theta_1) - \sin\theta_7 \cdot (\cos\theta_1 \cdot \cos\theta_6 - \sin\theta_1 \cdot \sin\theta_6), \\ o_z = 0, \\ a_x = 0, \\ a_y = 0, \\ a_z = 1, \\ p_x = a_1 \cdot \cos\theta_1 - a_3 \cdot (\cos\theta_1 \cdot \sin\theta_6 + \cos\theta_6 \cdot \sin\theta_1) - a_2 \cdot \sin\theta_1, \\ p_y = a_3 \cdot (\cos\theta_1 \cdot \cos\theta_6 - \sin\theta_1 \cdot \sin\theta_6) + a_2 \cdot \cos\theta_1 + a_1 \cdot \sin\theta_1, \\ p_z = d. \end{cases} \tag{6}$$

The value of each element in the coordinate system 6 is expressed as

$$\begin{cases} n_x = \sin\theta_5 \cdot (\sin\theta_1 \cdot \sin\theta_4 - \cos\theta_1 \cdot \cos\theta_4) - \cos\theta_5 \cdot (\cos\theta_1 \cdot \sin\theta_4 + \sin\theta_1 \cdot \cos\theta_4), \\ n_y = -\cos\theta_5 \cdot (\sin\theta_1 \cdot \sin\theta_4 - \cos\theta_1 \cdot \cos\theta_4) - \sin\theta_5 \cdot (\cos\theta_1 \cdot \sin\theta_4 + \cos\theta_4 \cdot \sin\theta_1), \\ n_z = 0, \\ o_x = \cos\theta_5 \cdot (\sin\theta_1 \cdot \sin\theta_4 - \cos\theta_1 \cdot \cos\theta_4) + \sin\theta_5 \cdot (\cos\theta_1 \cdot \sin\theta_4 + \cos\theta_4 \cdot \sin\theta_1), \\ o_y = \sin\theta_5 \cdot (\sin\theta_1 \cdot \sin\theta_4 - \cos\theta_1 \cdot \cos\theta_4) - \cos\theta_5 \cdot (\cos\theta_1 \cdot \sin\theta_4 + \sin\theta_1 \cdot \cos\theta_4), \\ o_z = 0, \\ a_x = 0, \\ a_y = 0, \\ a_z = 1, \\ p_x = a_1 \cdot \cos\theta_1 - a_3 \cdot (\cos\theta_1 \cdot \sin\theta_4 + \cos\theta_4 \cdot \sin\theta_1) + a_2 \cdot \sin\theta_1, \\ p_y = -a_3 \cdot (\sin\theta_1 \cdot \sin\theta_4 - \cos\theta_1 \cdot \cos\theta_4) - a_2 \cdot \cos\theta_1 + a_1 \cdot \sin\theta_1, \\ p_z = 0. \end{cases} \tag{7}$$

The value of each element in the coordinate system 10 is expressed as.

$$\begin{cases} n_x = \sin\theta_9 \cdot (\sin\theta_1 \cdot \sin\theta_8 - \cos\theta_1 \cdot \cos\theta_8) - \cos\theta_9 \cdot (\cos\theta_1 \cdot \sin\theta_8 + \sin\theta_1 \cdot \cos\theta_8), \\ n_y = -\cos\theta_9 \cdot (\sin\theta_1 \cdot \sin\theta_8 - \cos\theta_1 \cdot \cos\theta_8) - \sin\theta_9 \cdot (\cos\theta_1 \cdot \sin\theta_8 + \cos\theta_8 \cdot \sin\theta_1), \\ n_z = 0, \\ o_x = \cos\theta_9 \cdot (\sin\theta_1 \cdot \sin\theta_8 - \cos\theta_1 \cdot \cos\theta_8) + \sin\theta_9 \cdot (\cos\theta_1 \cdot \sin\theta_8 + \cos\theta_8 \cdot \sin\theta_1), \\ o_y = \sin\theta_9 \cdot (\sin\theta_1 \cdot \sin\theta_8 - \cos\theta_1 \cdot \cos\theta_8) - \cos\theta_9 \cdot (\cos\theta_1 \cdot \sin\theta_8 + \sin\theta_1 \cdot \cos\theta_8), \\ o_z = 0, \\ a_x = 0, \\ a_y = 0, \\ a_z = 1, \\ p_x = a_1 \cdot \cos\theta_1 - a_3 \cdot (\cos\theta_1 \cdot \sin\theta_8 + \cos\theta_8 \cdot \sin\theta_1) + a_2 \cdot \sin\theta_1, \\ p_y = -a_3 \cdot (\sin\theta_1 \cdot \sin\theta_8 - \cos\theta_1 \cdot \cos\theta_8) - a_2 \cdot \cos\theta_1 + a_1 \cdot \sin\theta_1, \\ p_z = d. \end{cases} \tag{8}$$

3. Numerical Simulation Verification

The mathematical model of the TCR is built using the Robotics Toolbox in MATLAB software [26]. With the help of the completed kinematic model, the mathematical model of the TCR is constructed based on the *D-H* parameterization method, where the linking rods of the robot arm have a linking function and are connected in a serial linking function.

As shown in Figures 3 and 4, the mathematical model of the initial state of TCR is established through the Robotic Toolbox in MATLAB software. To simulate and verify the forward kinematics of TCR, take any set of joint angles theta = $[0, \pi/2, \pi/4, \pi/4]$ and substitute it into equation (3), which is expressed as follows:

$${}^{0}_{4}T = \begin{bmatrix} -1 & 0 & 0 & 0.0654 \\ 0 & -1 & 0 & 0.1631 \\ 0 & 0 & 1 & 0 \\ 0 & 0 & 0 & 1 \end{bmatrix}, \tag{9}$$

where the MATLAB output matrix is

$$T = \begin{bmatrix} -1 & 0 & 0 & 0.0654 \\ 0 & -1 & 0 & 0.1631 \\ 0 & 0 & 1 & 0 \\ 0 & 0 & 0 & 1 \end{bmatrix}. \tag{10}$$

Three sets of joint angles theta = $[0, \pi/2, 3\pi/4, -\pi/2]$, theta = $[0, \pi/2, \pi/4, \pi/4]$, theta = $[0, \pi/2, 3\pi/4, -\pi/2]$ are introduced and brought into equation (4), and the corresponding verification results are consistent with equations (9) and (10), which in turn argue that the positive kinematic equations of the TCR are correct.

The boundary of the open space of the manipulator is not a regular outer contour, and to simplify the analysis, it is decomposed into several rectangles. The manipulator is reduced to linkage joints, and a joint coordinate system is established at the axes of the large and small arms. When solving for the spatial pose of a point, the relative relationship between each link and the kinematics is solved in the form of an isomorphic transformation of its relative motion to the previous link. The coordinate system of the arm of the TCR manipulator is shown in Figure 5. The link parameters of the robotic arm are indicated in Table 2.

Assuming that a rigid body needs to be considered for motion, rotation, and the coexistence of motion and rotation

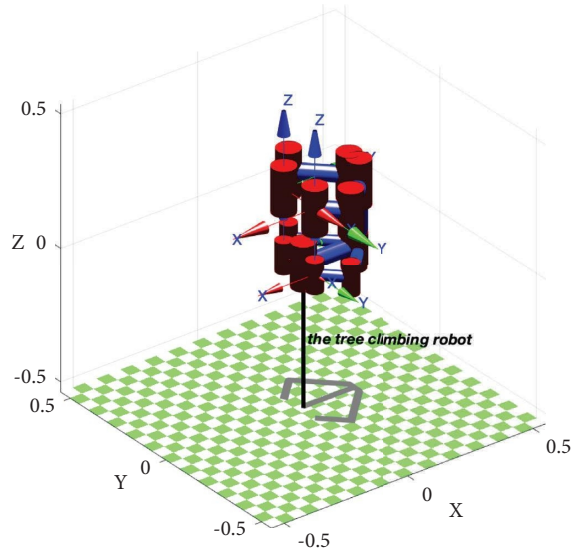

Figure 3: Schematic diagram of initial position of TCR.

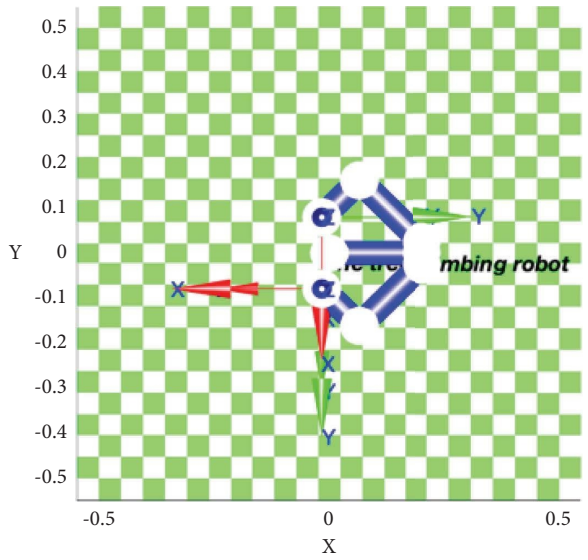

Figure 4: Schematic diagram of initial posture of TCR.

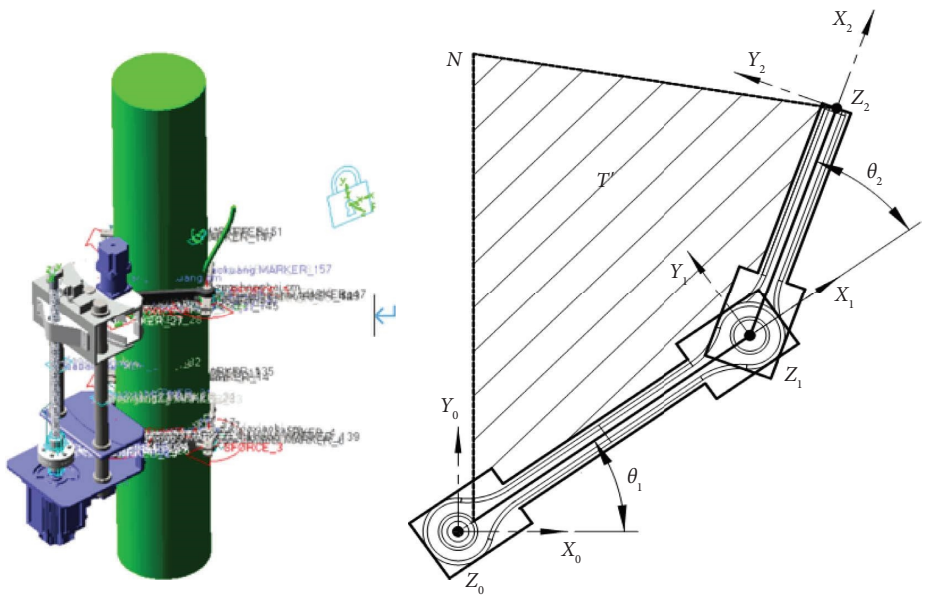

Figure 5: The coordinate system of the robotic arm.

Table 2: The link parameters of robotic arm.

i	a_{i-1}	α_{i-1}	d_i	θ_i
1	0	0	0	θ_1
2	L	0	0	θ_2

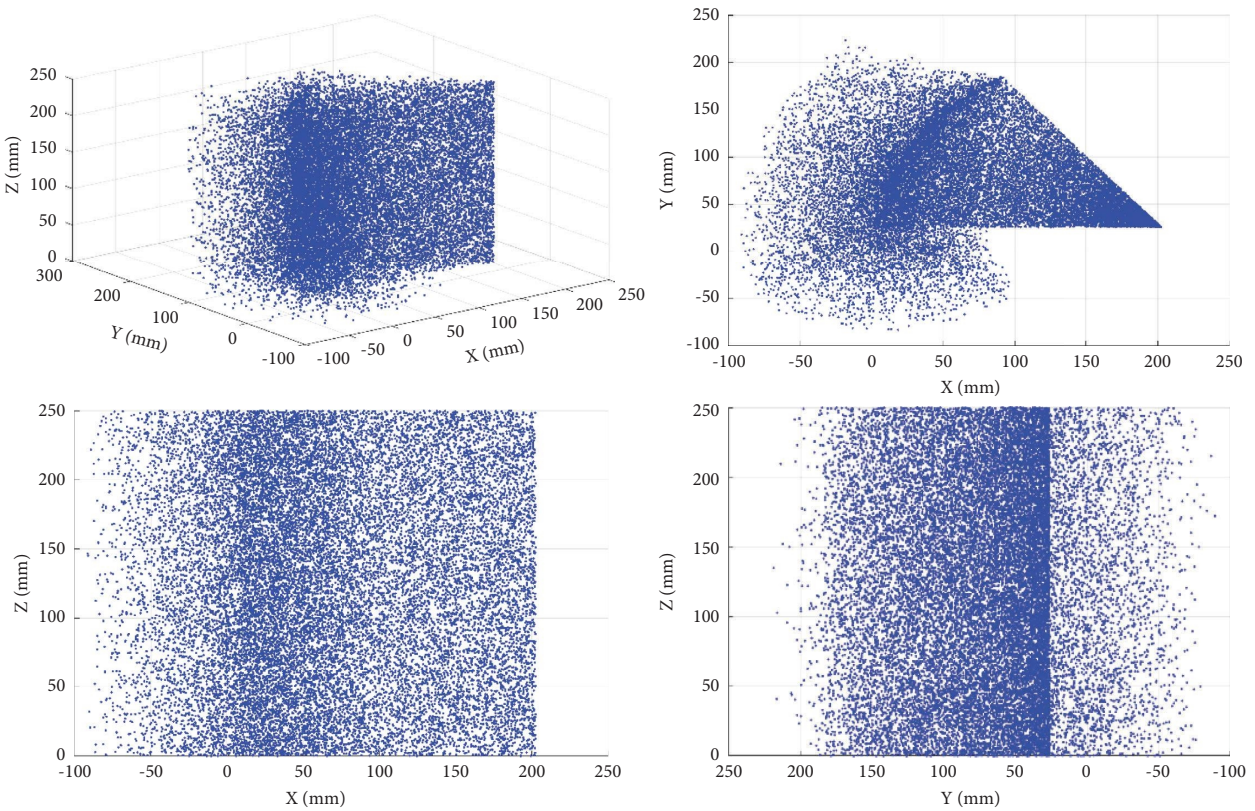

Figure 6: The feasible workspace of the arm of TCR.

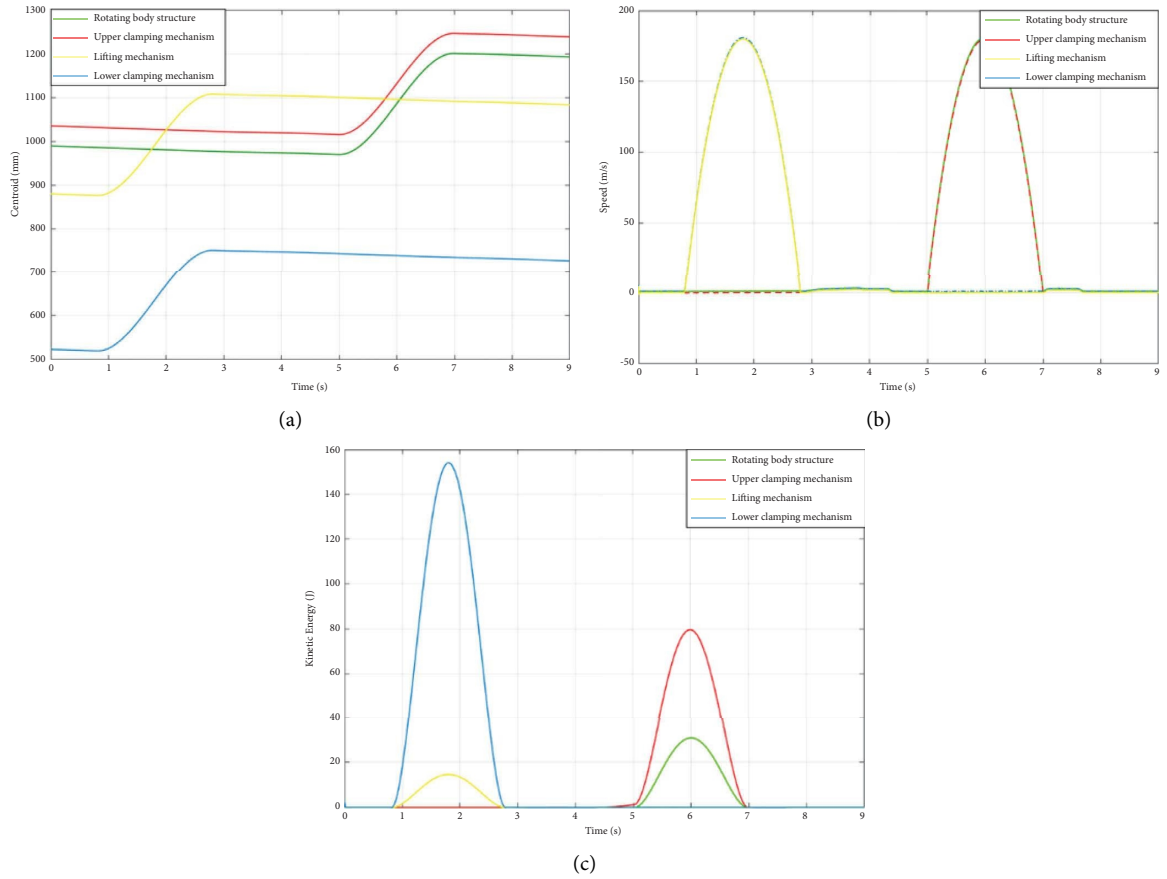

Figure 7: Centroid, velocity, and kinetic energy changes of each part. (a) Centroid changes. (b) Speed changes. (c) Kinetic energy changes.

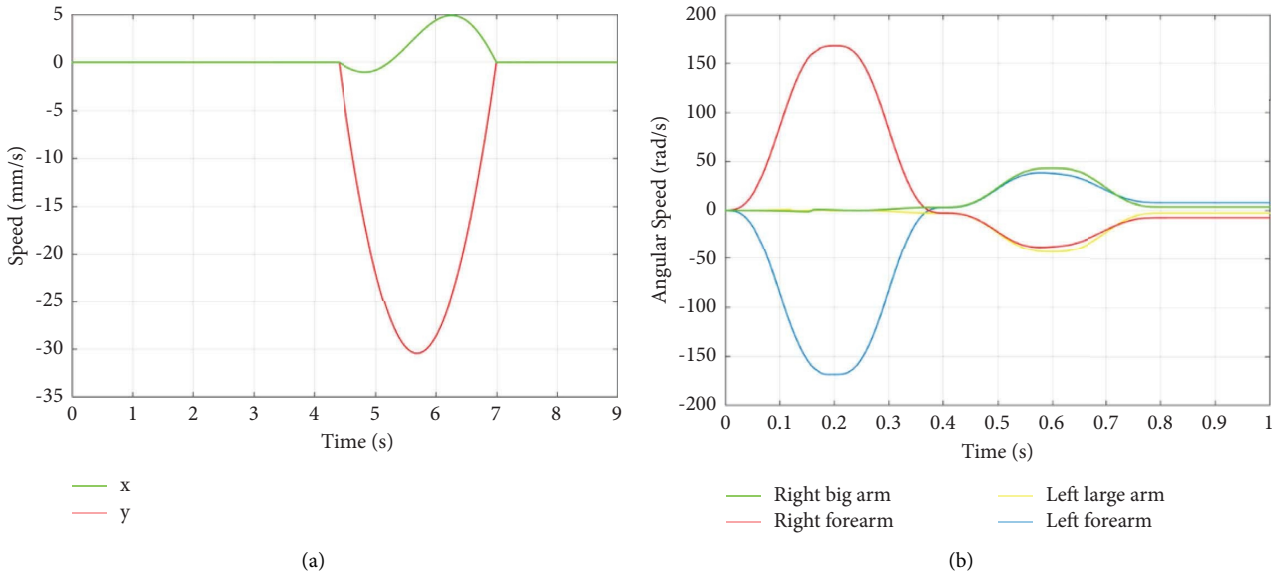

Figure 8: Centroid, velocity, and kinetic energy changes of each part. (a) Climbing velocity variation curves. (b) Angular speed of the robot arm rotating around the Z-axis.

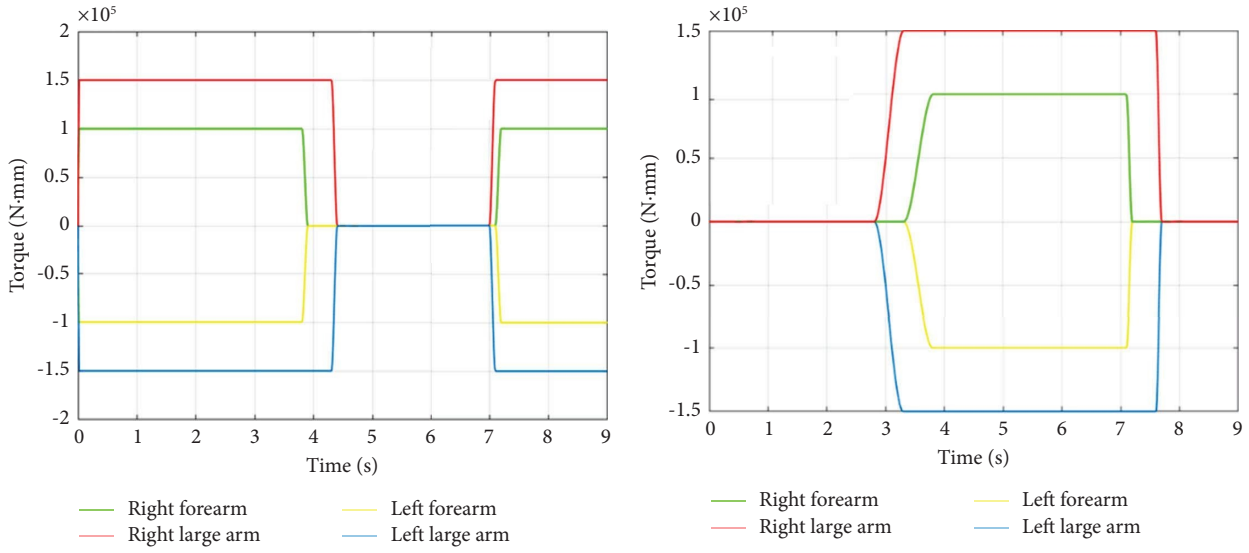

Figure 9: Torque time characteristic curves of the upper and lower robot arms of the TCR around the Z-axis. (a) Torque-time characteristic curve of the upper robot arm around the Z-axis. (b) Torque-time characteristic curve of the lower robot arm around the Z-axis.

in space, the D-H transformation matrix of the adjacent linked coordinate system is

$$
\begin{aligned}
{}_{i}^{i-1}T &= \mathrm{Rot}(z,\theta_n)\mathrm{Trans}(0,0,d_n)\mathrm{Trans}(a_n,0,0)\mathrm{Rot}(x,\alpha_n) \\
&= \begin{bmatrix} \cos\theta_n & -\sin\theta_n & 0 & 0 \\ \sin\theta_n & \cos\theta_n & 0 & 0 \\ 0 & 0 & 1 & 0 \\ 0 & 0 & 0 & 1 \end{bmatrix}\begin{bmatrix} 1 & 0 & 0 & 0 \\ 0 & 1 & 0 & 0 \\ 0 & 0 & 1 & d_n \\ 0 & 0 & 0 & 1 \end{bmatrix}\begin{bmatrix} 1 & 0 & 0 & a_n \\ 0 & 1 & 0 & 0 \\ 0 & 0 & 1 & 0 \\ 0 & 0 & 0 & 1 \end{bmatrix}\begin{bmatrix} 1 & 0 & 0 & 0 \\ 0 & \cos\alpha_n & -\sin\alpha_n & 0 \\ 0 & \sin\alpha_n & \cos\alpha_n & 0 \\ 0 & 0 & 0 & 1 \end{bmatrix} \\
&= \begin{bmatrix} \cos\theta_n & -\sin\theta_n\cos\alpha_n & \sin\theta_n\sin\alpha_n & a_n\cos\theta_n \\ \sin\theta_n & \cos\theta_n\cos\alpha_n & -\cos\theta_n\sin\alpha_n & a_n\sin\theta_n \\ 0 & \sin\alpha_n & \cos\alpha_n & d_n \\ 0 & 0 & 0 & 1 \end{bmatrix}.
\end{aligned} \tag{11}
$$

All edge segments of the end effector are defined as sets.

$$
\xi_{T'} = \xi_{T_1'} \cup \xi_{T_2'} = \left\{ \begin{matrix} CD, DI, IJ, JF, FE, EG, GH, HC, \\ LM, MN, NO, OP, PQ, QR, RS, ST, TU, UV, VW \end{matrix} \right\}. \tag{12}
$$

4. Dynamics Simulation Analysis

In order to verify the dynamic performance of TCR, dynamic simulation is carried out using ADAMS and SolidWorks analysis tools. The model of TCR is established in SolidWorks and imported into ADAMS. Because the 3D model of TCR is too complex, it is necessary to simplify the model by removing unimportant parts and combining some relatively static parts into a whole to improve the running speed of ADAMS. After preprocessing, the simulated TCR is run from the initial position to the final position. The feasible workspace for solving with MATLAB is shown in Figure 6.

The kinematics and dynamics of the crawling process of the TCR virtual prototype were simulated by ADAMS. Figure 7 reveals the position, trajectory, velocity, acceleration, angle, angular velocity, angular acceleration, and the variation curves of the momentum, kinetic energy, and gravitational potential energy and the changes involved for the center of mass or any point of the TCR structure.

In Figure 7, the centers of the gravity-time characteristic curve, velocity-time characteristic curve, and translation amount-time characteristic curve are measured within 9.0 s, and the regularity is found to be summarized. The upper and lower structures move asynchronously. Starting from 0.8 s, the lifting structure and the lower clamping structure first move upwards, stopping at 2.8 s, and starting at 5.0 s, the upper clamping structure and the rotating body structure start to rise. Figure 8 reflects the time-varying pattern of different climbing speeds and the angular velocity variation profile of the TCR robot arm rotating around the Z-axis during the TCR climbing movement.

In Figure 8, the characteristic curves of displacement and velocity versus time at the center point of the clamping structure along the x and y directions are measured. In summary, the rotational movement of the body produces a certain degree of displacement in the x and y directions, and due to the installation of a rotating motor in the clamping structure, the overall structure is not completely symmetrical, and there is an abrupt change in the center of mass and velocity change curve along the y direction.

Figure 9 describes the torque time characteristic curve of the upper robot arm of the TCR around the Z-axis and the torque time characteristic curve of the lower robot arm of the TCR around the Z-axis during the dynamic climbing motion of the TCR.

In Figure 9, the characteristic curves of the angular velocity, torque, and time of rotation of the robotic arm are measured. The gripping and releasing action of the robotic arm is the core action of the robot, and the dynamic analysis above reveals that the torque of the large and small arms of the robotic arm is not simultaneously zero, which is the same as the validation results.

5. Conclusions

This paper presents a tree-climbing robot with variable diameters and rotatable obstacles. The kinematic model of the TCR is described by an improved D-H parametric method, and the kinematic equations of the TCR robot are solved and verified to be correct.

(1) The mathematical analysis model of the TCR is created using the Robotics Toolbox in MATLAB, and the realistic feasibility is verified by simulating the kinematic equations proposed in the paper.

(2) ADAMS is introduced to simulate and analyse the kinematics and dynamics of the climbing process on the TCR. The simulations verify the rationality and feasibility of the gait planning during the tree climbing process of the TCR, and the time-characteristic variation curves of each physical quantity and each structural joint are generated in the postprocessing module of the TCR structure.

(3) The analysis of the reachable area of the robot arm workspace is described in conjunction with MATLAB, and the relevant kinematic parameter variation patterns, such as robot torque, contact force, center of mass displacement, velocity, acceleration, angular velocity, and angular acceleration, are revealed in ADAMS.

Data Availability

No data were used to support the findings of this study.

Conflicts of Interest

The authors declare that they have no conflicts of interest regarding the publication of this paper.

Acknowledgments

The authors thank the Northeast Forestry University (NEFU), Heilongjiang Institute of Technology (HLJIT) and Huaqiao University for their support. The research topic was supported by the 2022 Heilongjiang Provincial Key Research and Development Plan Key Area Special Project (SC2022ZX01A0052, Xigui Wang, NEFU), the Innovation Foundation for Doctoral Program of Forestry Engineering of Northeast Forestry University (grant no. 000/4111410203, Jie Tang, NEFU), the Doctoral Research Startup Foundation Project of Heilongjiang Institute of Technology (grant no. 2020BJ06, Yongmei Wang, HLJIT), the Natural Science Foundation Project of Heilongjiang Province (grant no. LH2019E114, Baixue Fu, HLJIT), the Basic Scientific Research Business Expenses (Innovation Team Category) Project of Heilongjiang Institute of Engineering (grant no. 2020CX02, Baixue Fu, HLJIT), the Special Project for Double First-Class-Cultivation of Innovative Talents (grant no. 000/41113102, Jiafu Ruan, NEFU), the Youth Science Fund of Heilongjiang Institute of Technology (grant no. 2015QJ02), and the Fundamental Research Funds for the Central Universities (grant no. 2572016CB15).

References

[1] D. Ren, S. Yang, G. Yan, and Y. Zhang, "Study on a novel wheel type tree-climbing robot," in *Proceedings of the 2014 Seventh International Symposium on Computational Intelligence and Design*, pp. 150–153, Hangzhou, China, December 2014.

[2] T. L. Lam and Y. S. Xu, "A review on path planning and obstacle avoidance algorithms for autonomous mobile robots," *Journal of Robotics*, vol. 2022, Article ID 2538220, 14 pages, 2022.

[3] P. Sudhakara, V. Ganapathy, B. Priyadharshini, and K. Sundaran, "Obstacle avoidance and navigation planning of a wheeled mobile robot using amended artificial potential field method," *Procedia Computer Science*, vol. 133, pp. 998–1004, 2018.

[4] A. Hentout, A. Maoudj, and M. Aouache, "A review of the literature on fuzzy-logic approaches for collision-free path planning of manipulator robots," *Artificial Intelligence Review*, 2022.

[5] Y. H. Bai, M. Z. Luo, and F. L. Pang, "An algorithm for solving robot inverse kinematics based on FOA optimized BP neural network," *Applied Sciences*, vol. 11, no. 15, 2021.

[6] L. Wu, Q. Liu, X. Tian, J. Zhang, and W. Xiao, "A new improved fruit fly optimization algorithm IAFOA and its application to solve engineering optimization problems," *Knowledge-Based Systems*, vol. 144, pp. 153–173, 2018.

[7] H. Ren and P. Ben-Tzvi, "Learning inverse kinematics and dynamics of a robotic manipulator using generative adversarial networks," *Robotics and Autonomous Systems*, vol. 124, Article ID 103386, 2020.

[8] H. Ye, D. Wang, J. Wu, Y. Yue, and Y. L. Zhou, "Forward and inverse kinematics of a 5-DOF hybrid robot for composite material machining," *Robotics and Computer-Integrated Manufacturing*, vol. 65, Article ID 101961, 2020.

[9] L. Q. Zhou, J. An, R. H. Zhao, and H. R. Mu, "Trajectory planning and simulation of industrial robot based on MATLAB and robot studio," in *Proceedings of the IEEE 4th International Conference on Electronics Technology (ICET)*, pp. 910–914, Chengdu, China, May 2021.

[10] S. Dereli and R. Köker, "Calculation of the inverse kinematics solution of the 7-DOF redundant robot manipulator by the firefly algorithm and statistical analysis of the results in terms of speed and accuracy," *Inverse Problems in Science and Engineering*, vol. 28, no. 5, pp. 601–613, 2020.

[11] Y. J. Li, W. Wei, Y. Gao, D. L. Wang, and Z. Fan, "Pq-rrt∗: an improved path planning algorithm for mobile robots," *Expert Systems with Applications*, vol. 152, Article ID 113425, 2020.

[12] H. J. Wang, Y. Y. Lin, X. J. Xu, Z. Y. Chen, Z. H. Wu, and Y. C. Tang, "A study on long-close distance coordination control strategy for litchi picking," *Agronomy*, vol. 12, no. 7, 2022.

[13] C. Lopez-Franco, J. Hernandez-Barragan, A. Y. Alanis, and N. Arana-Daniel, "A soft computing approach for inverse kinematics of robot manipulators," *Engineering Applications of Artificial Intelligence*, vol. 74, pp. 104–120, 2018.

[14] I. Pikalov, E. Spirin, M. Saramud, and M. Kubrikov, "Vector model for solving the inverse kinematics problem in the system of external adaptive control of robotic manipulators," *Mechanism and Machine Theory*, vol. 174, Article ID 104912, 2022.

[15] M. Y. Chen, Y. C. Tang, X. J. Zou et al., "Three-dimensional perception of orchard banana central stock enhanced by adaptive multi-vision technology," *Computers and Electronics in Agriculture*, vol. 174, Article ID 105508, 2020.

[16] G. C. Lin, L. X. Zhu, J. H. Li, X. J. Zou, and Y. C. Tang, "Collision-free path planning for a guava-harvesting robot based on recurrent deep reinforcement learning," *Computers and Electronics in Agriculture*, vol. 188, Article ID 106350, 2021.

[17] O. El Baji, N. Ben Said Amrani, and D. Sarsri, "Online trajectory tracking control based on the explicit form of the equations of motion for serial manipulator using the new formulation," *Journal of Robotics*, vol. 2022, Article ID 8715161, 14 pages, 2022.

[18] Y. Wang, D. Liu, H. M. Zhao et al., "Rapid citrus harvesting motion planning with pre-harvesting point and quad-tree," *Computers and Electronics in Agriculture*, vol. 202, Article ID 107348, 2022.

[19] L. Ye, J. L. Duan, Z. Yang, X. J. Zou, M. Y. Chen, and S. Zhang, "Collision-free motion planning for the litchi-picking robot," *Computers and Electronics in Agriculture*, vol. 185, Article ID 106151, 2021.

[20] W. Z. Liu, C. Zhao, Y. Liu, H. W. Wang, W. Zhao, and H. M. Zhang, "Sim2real kinematics modeling of industrial robots based on FPGA-acceleration," *Robotics and Computer-Integrated Manufacturing*, vol. 77, Article ID 102350, 2022.

[21] J. K. Wang, B. P. Li, and M. Q.-H. Meng, "Kinematic constrained Bi-directional RRT with efficient branch pruning for robot path planning," *Expert Systems with Applications*, vol. 170, Article ID 114541, 2021.

[22] M. L. Kang, Z. M. Fan, X. J. Yu et al., "Division-merge based inverse kinematics for multi-DOFs humanoid robots in unstructured environments," *Computers and Electronics in Agriculture*, vol. 198, Article ID 107090, 2022.

[23] H. Wang, C. J. Hohimer, S. Bhusal, M. Karkee, C. K. Mo, and J. H. Miller, "Simulation as a tool in designing and evaluating a robotic apple harvesting system," *IFAC-PapersOnLine*, vol. 51, no. 17, pp. 135–140, 2018.

[24] X. B. Zhang, J. G. Liu, and Y. M. Li, "Research on simulation system for human-SRL collaborative motion planning," *Journal of Robotics*, vol. 2022, Article ID 7561891, 14 pages, 2022.

[25] F. C. Sun, Y. Chen, Y. Y. Wu, L. X. Li, and X. L. Ren, "Motion planning and cooperative manipulation for mobile robots with dual arms," *IEEE Transactions on Emerging Topics in Computational Intelligence*, vol. 6, no. 6, pp. 1345–1356, 2022.

[26] X. M. Cao, X. J. Zou, C. Y. Jia, M. Y. Chen, and Z. Q. Zeng, "Rrt-based path planning for an intelligent litchi-picking manipulator," *Computers and Electronics in Agriculture*, vol. 156, pp. 105–118, 2019.